

Intrinsic electrocaloric effect in ferroelectric alloys from atomistic simulations

S. Lisenkov* and I. Ponomareva

Department of Physics, University of South Florida, Tampa, Florida 33620, USA

(Received 10 September 2009; published 28 October 2009)

Electrocaloric effect (ECE) in $(\text{Ba}_{0.5}\text{Sr}_{0.5})\text{TiO}_3$ ferroelectric alloys is calculated from first principles using a computational scheme that combines canonical and microcanonical Monte Carlo simulations. Our results are in very good agreement with the available experimental data and reveal many intriguing features of ECE including; (i) a significant enhancement of the ECE in paraelectric phase, (ii) nearly linear reversible temperature change associated with the electric field variation up to extremely large fields and, (iii) a possibility of achieving large ECE at room temperatures. Our atomistic insight suggests that in ferroelectrics ECE is caused by the redistribution of the entropy between the part associated with the dipoles' order and the part associated with the order in the kinetic energies of atomic vibrations. This mechanism can also be viewed as a "conversion" of spatially inhomogeneous dipole distribution into spatially inhomogeneous temperature distribution.

DOI: [10.1103/PhysRevB.80.140102](https://doi.org/10.1103/PhysRevB.80.140102)

PACS number(s): 77.70.+a, 31.15.A-, 77.80.Bh, 77.84.Dy

Electrocaloric effect (ECE) in ferroelectrics is experiencing a renaissance thanks to the recent reports of large electrocaloric response in ferroelectric thin films¹ and polymers.² ECE is measured by a reversible change in the temperature under either application or removal of the electric field and has great potential for application in refrigeration technology. The earlier data on ECE reported only a slight variation in temperature as a function of the electric field variation³⁻⁶ resulting in diminished interest in this phenomenon. However, the recent groundbreaking reports of the large temperature response (≈ 12 K) to the electric field variation in ferroelectric thin films¹ and polymers² has provided a revived impetus to this phenomena. Despite these exciting developments, the mechanism responsible for ECE remain unsolved.¹ Specifically, many questions need to be answered. Does the ECE occur only above paraelectric to ferroelectric phase transition or below such transition or both below and above this transition? Is the effect larger in paraelectric or ferroelectric phase? In what materials the electrocaloric coefficient peaks near the room temperature? What is the atomistic mechanism responsible for ECE? Answers to these questions require detailed investigations using accurate theoretical methods. Important insights into intrinsic ECE in BaTiO_3 were reported in theoretical work by Akcay *et al.*⁷ where the intrinsic ECE in bulk BaTiO_3 was studied using a phenomenological model and Maxwell relations. It was found that the adiabatic temperature change of 8 K can be achieved in this material, thanks to the disappearance of the discontinuity in the ferroelectric phase transition due to the electric field application. Another work⁸ reported an electrocaloric coefficient of 0.52×10^{-7} Km/V in $\text{Pb}(\text{Zr}_{0.4}\text{Ti}_{0.6})\text{O}_3$ bulk and nanodot from first-principles-based simulations. In this work classical molecular dynamics simulations were performed using a first-principles-derived effective Hamiltonian to demonstrate that ECE can occur even at GHz frequencies.

In this Rapid Communication, we propose an alternative computational scheme that allows accurate atomistic simulations of ECE from first principles. Among different ferroelectric alloys the $(\text{Ba}_x\text{Sr}_{1-x})\text{TiO}_3$ alloys may be excellent candidates for applications that exploit ECE since the ferroelectric transition temperature (T_C) in such alloys changes

almost linearly with Ba concentration (from 400 K for pure BaTiO_3 down to 80 K in $\text{Ba}_{0.1}\text{Sr}_{0.9}\text{TiO}_3$). They also exhibit a wide range of phase transitions. In fact, these alloys undergo three phase transitions as the temperature is decreased: paraelectric cubic to ferroelectric tetragonal, tetragonal to orthorhombic and, orthorhombic to rhombohedral. Here we focus on $(\text{Ba}_{0.5}\text{Sr}_{0.5})\text{TiO}_3$ (BST) alloys since its $T_C=250$ K is just below the room temperature and it is also a good representative of other $(\text{Ba}_x\text{Sr}_{1-x})\text{TiO}_3$ alloys. Our results suggest that a very large intrinsic ECE can be achieved at room temperature in BST alloys, and we also provide answers to the important questions raised above.

We begin by considering four atomic configurations of BST alloys and label them BST-1, BST-2, BST-3, and BST-4 to be described in detail below. Configuration BST-1 corresponds to disordered $(\text{Ba}_{0.5}\text{Sr}_{0.5})\text{TiO}_3$ solid solution with Sr and Ba atoms distributed randomly. Configuration BST-2 has a smooth compositional gradient with its Ba concentration increasing by 1% in each successive layer. In this configuration the minimum Ba concentration is 40% (bottom layer) and the maximum Ba concentration is 60% (top layer). Configuration BST-3 has a "superlattice" structure with a periodicity of 21 layers so that each seven layers have different Ba concentration. This configuration can be expressed as $[(\text{Ba}_{0.4}\text{Sr}_{0.6})\text{TiO}_3]_7/[(\text{Ba}_{0.5}\text{Sr}_{0.5})\text{TiO}_3]_7/[(\text{Ba}_{0.6}\text{Sr}_{0.4})\text{TiO}_3]_7$, where index 7 indicates the number of layers with the alloy composition given in the square brackets. Similarly, configuration BST-4 also corresponds to a "superlattice" structure and can be written as $[(\text{Ba}_{0.3}\text{Sr}_{0.7})\text{TiO}_3]_7/[(\text{Ba}_{0.5}\text{Sr}_{0.5})\text{TiO}_3]_7/[(\text{Ba}_{0.7}\text{Sr}_{0.3})\text{TiO}_3]_7$. Note, that all these alloys have the same average concentration of Ba (50%) and same T_C as obtained from our computations. They are modeled by $12 \times 12 \times 21$ supercell (15 120 atoms) which is periodic along all three directions to simulate the bulk system.⁹ The total energy of this supercell is given by the first-principles-based effective Hamiltonian

$$\begin{aligned}
 E_{tot} = & E_{self}(\{\mathbf{u}_i\}) + E_{dpl}(\{\mathbf{u}_i\}) + E_{short}(\{\mathbf{u}_i\}) + E_{elas}(\{\mathbf{v}_i\}, \eta_H) \\
 & + E_{int}(\{\mathbf{u}_i\}, \{\mathbf{v}_i\}, \eta_H) + E_{loc}(\{\mathbf{u}_i\}, \{\mathbf{v}_i\}, \{\sigma_i\}, \{\eta_{loc,i}\}) \\
 & + E_{elec}(\{\mathbf{u}_i\}), \quad (1)
 \end{aligned}$$

where \mathbf{u}_i is the local soft mode at the site i of the supercell (the product of \mathbf{u}_i with the Born effective charge yields the electrical dipole moment at site i) and \mathbf{v}_i is a dimensionless vector related to the inhomogeneous strain around this site, while η_H is the homogeneous strain tensor. $\{\sigma_i\}$ characterizes the alloy configuration, while $\eta_{loc,i}$ characterizes the strain resulting from the difference in ionic size between Ba and Sr atoms.¹⁰ E_{tot} includes a local mode self energy, E_{self} (harmonic and unharmonic contributions), a long-range dipole-dipole interaction, E_{dpl} , a short-range interaction between local modes, E_{short} , an elastic energy, E_{elas} , interaction between the local modes and strains, E_{int} , interactions responsible for alloying effects, E_{loc} , and an interaction of the local modes with electric field, E_{elec} .¹¹ This Hamiltonian correctly reproduces the complex sequence of phase transitions in BST alloys for a very wide compositional range¹² and has been used to study a wide range of ferroelectric alloy properties yielding results in good agreement with both experiment and first-principles calculations (see Refs. 10 and 13–16). We use this Hamiltonian for studying ECE by incorporating both canonical and microcanonical Monte Carlo (MC) simulations. The simulation approach uses a two step process. The first step involves conducting MC simulations at a constant temperature using Metropolis algorithm¹⁷ (canonical ensemble). We use typically 150 000 MC sweeps in this step to equilibrate the system at the desired temperature and 150 000 MC sweeps to collect averages. No electric field is applied at this step. At the second step we switch to simulations at a constant total energy (Creutz algorithm¹⁸ for microcanonical simulations) and apply dc electric field. At this step we first allow the system to reach a new equilibrium under electric field using 150 000 MC sweeps and then the subsequent 150 000 MC sweeps are used to calculate ΔT associated with the electric field applied. In the simulations the temperature is calculated as $T = \langle E_d \rangle / k_B$, where $\langle E_d \rangle$ is the average demon energy¹⁸ (the energy absorbed during simulations by an extra degree of freedom—“demon”— and analogous to the kinetic energy carried by the conjugate momenta in the microcanonical formulations) and k_B is the Boltzmann constant. For given effective Hamiltonian the error bar for the temperatures is ± 0.5 K. Note that in ferroelectric phase the electric field is applied along the polarization direction. This approach allows one to compute ΔT directly from first principles without resorting to the use of Maxwell equations and/or introducing empirical parameters.

To test our computational technique we first study the change in temperature under a change in the applied electric field of 500 kV/cm (see Fig. 1). The maximum change in the temperature $\Delta T = 17$ K is in agreement with the experimentally found 12 K for $\text{Pb}(\text{Zr}_{0.95}\text{Ti}_{0.05})\text{O}_3$ thin films under similar change in the electric field.¹ Our simulations also correctly reproduce the overall dependence of ΔT on T reported in Refs. 1, 2, and 7 with the peak in the ΔT occurring near T_C . Interestingly, our simulations demonstrate an asymmetry in the $\Delta T(T)$ with respect to T_C with ΔT being much higher in the paraelectric phase for the chosen ΔE . We did not find any dependence of the ECE on the alloy configurations for the four configurations considered.

Next we study the dependence of ΔT on ΔE . During these simulations the electric field is increased from 0 to 1000

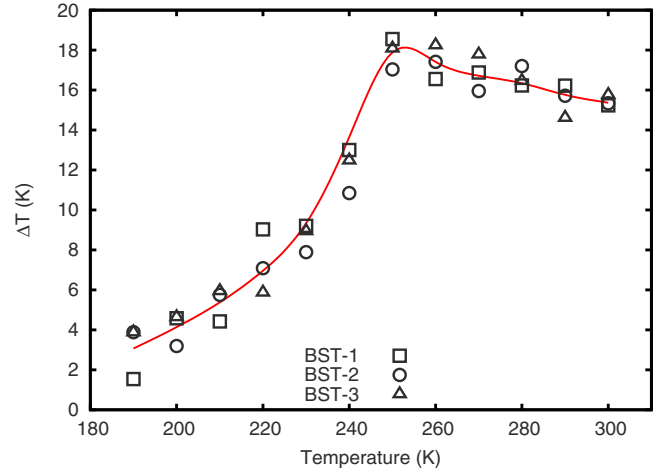


FIG. 1. (Color online) The change in the temperature ΔT achieved by an increase in electric field from 0 to 500 kV/cm as a function of temperature. We do not show the data for BST-4 since they are similar to the data for BST-3. Solid line is a guide to the eyes. Note, that we do not observe any dependence on the alloy configuration.

kV/cm in steps of 100 kV/cm and the data are obtained for the same temperatures as shown in Fig. 1. The computed change in the temperature for BST-1 is given in Fig. 2 for a few selected temperatures. Other temperatures (not shown) follow the same trends. We also conducted simulations at much higher fields (see the inset to Fig. 2). Interestingly, our results show two families of curves. One with a steep slope (corresponding to paraelectric phase) and another one with a moderate slope (corresponding to ferroelectric phase). Surprisingly, in paraelectric phase the dependence of ΔT on ΔE remains linear up to extremely high fields indicating that the electrocaloric coefficient depends only on $\Delta E = E_2 - E_1$ but not on the initial and final fields E_1 and E_2 , respectively. In

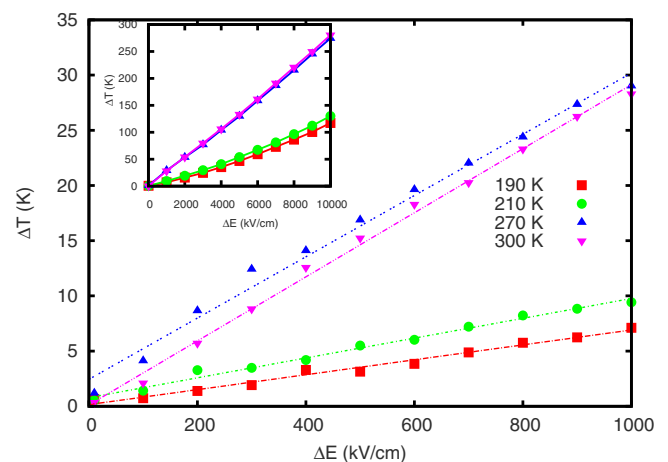


FIG. 2. (Color online) The change in the temperature ΔT as a function of ΔE for BST-1. Only two temperatures are shown in paraelectric phase (270 and 300 K) and ferroelectric phase (190 and 210 K). The solid lines correspond to the linear fit. The inset shows ΔT obtained at much larger ΔE . The solid lines on the inset correspond to the linear fit in paraelectric phase and quadratic fit in ferroelectric phase.

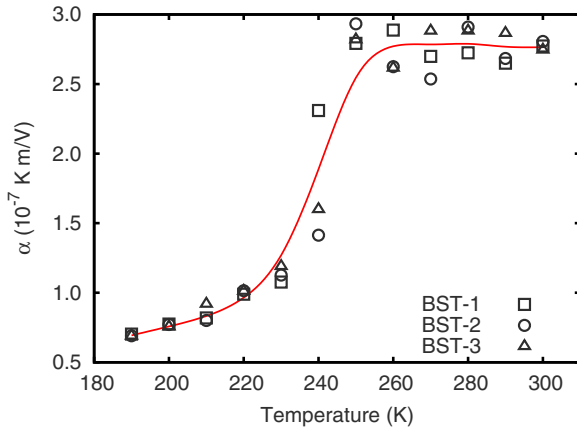


FIG. 3. (Color online) The slope $\alpha = \Delta T / \Delta E$ is given as a function of T for different alloy configurations. Solid line is a guide to the eye. The data for BST-4 are very similar to BST-3 and not shown here. No dependence of α on the alloy configuration is found.

the ferroelectric phase, however, we observe deviations from the linear behavior for fields 1000 kV/cm and higher that confirms the fact that in ferroelectric phase the ECE depends on both ΔE and E_1, E_2 as reported in Ref. 7. Note that ΔT reported here is reversible as verified in the additional set of calculations where the electric field was decreased. The data for other configurations (BST-2, BST-3 and BST-4) show similar behavior.

Next we report the dependence of the slope $\alpha = \Delta T / \Delta E$ on the temperature (see Fig. 3). This slope characterizes the strength of the electrocaloric coupling. From Fig. 3 one can see that α increases almost linearly in the ferroelectric phase as we approach T_C , then experiences a jump at T_C and remains nearly constant thereafter in the paraelectric phase. In ferroelectric phase our computed $\alpha = 0.67 \times 10^{-7}$ Km/V compares well with α in PZT alloys obtained from both experiment ($\alpha = 0.60 \pm 0.05 \times 10^{-7}$ Km/V) (Ref. 4) and computations ($\alpha = 0.52 \times 10^{-7}$ Km/V).⁸ Interestingly, α remains very high and nearly constant in the paraelectric phase up to room temperature. Thus, our results indicate that, while the ECE occurs in both ferroelectric and paraelectric phases, however, it is almost three times larger in paraelectric phase. These findings are in agreement with Jona and Shirane.¹⁹

We next investigate the atomistic mechanisms responsible for this behavior. The driving force for ECE is a change in entropy associated with the electric field variation. On atomistic level that corresponds to the realignment of the electric dipoles under an application or removal of electric field. For example, in paraelectric phase, and in the absence of electric field, the dipoles are completely disordered. Such disorder is associated with large entropy. When the electric field is applied the dipoles realign with the field resulting in the appearance of the induced polarization. This ordering also leads to a decrease in the entropy part associated with the dipoles' alignment that should be compensated by an increase in the temperature to keep the total entropy unchanged as dictated by reversible adiabatic conditions. As a quantitative measure of the dipoles' alignment with respect to the electric field, we can use the distribution of the dipoles over

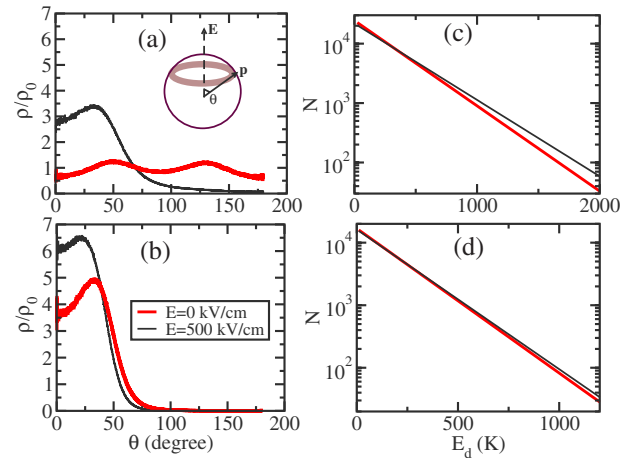


FIG. 4. (Color online) Simulations in BST-1 configuration under applied electric field of 500 kV/cm (thin line) and without electric field (thick line). In left panels the normalized dipole density is shown as a function of the angle θ between the dipole and the electric field as obtained from simulations at (a) $T=300$ K and (b) $T=190$ K. Inset to Fig. 4(a) shows schematization for ρ computations with the shaded area indicating the thin sphere segment ΔS that accommodates Δn dipoles. In right panels the distribution of the microcanonical demon energies (E_d) over the last 150 000 MC sweeps is shown as obtained from simulations at (a) $T=300$ K and (b) $T=190$ K.

the angles θ ; the angles between a given dipole p and the electric field E . Here we chose to plot the normalized dipole density (ρ / ρ_0) as a function of θ . ρ can be computed as $\rho = \Delta n / \Delta S$, where Δn is the total number of dipoles pointing inside a thin sphere segment ΔS in the vicinity of θ [see inset to Fig. 4(a)]. Normalization is done with respect to the density of dipoles (ρ_0) uniformly distributed within a unit sphere. Such an uniform distribution is a characteristic of a complete disorder. Note that in our notation a system of completely disordered dipoles will have $\rho(\theta) / \rho_0 = 1$. On the other hand, a completely ordered system with all the dipoles pointing along the electric field is characterized by $\rho(\theta) / \rho_0 = \delta(\theta)$. Figure 4(a) shows $\rho(\theta) / \rho_0$ at $T=300$ K (paraelectric phase) for zero electric field (thick red line) and field of 500 kV/cm (thin black line). At zero field the dipoles are almost homogeneously distributed over θ indicating a disordered state of the system. The two small peaks in the density correspond to the preferred [111] direction for the dipoles as dictated by the effective Hamiltonian (see Ref. 15 for the discussion on the preferred directions). Application of the electric field results in a drastic change in the dipoles' ordering [see the thin black line in Fig. 4(a)] that leads to: (1) strong asymmetry in the density function; (2) a threefold increase in the dipoles' density near the field direction; (3) disappearance of the dipoles pointing against the direction of the electric field. This drastic increase in the ordering leads to an entropy decrease. Where does the excess entropy go? To answer this question we plot the distributions of microcanonical demon energies¹⁸ for the same electric fields [see Fig. 4(c)]. In our computations the demon energy is related to the kinetic energy of the local mode or kinetic energy associated with the atomic vibrations in a unit cell. From Fig.

4(c) it can be seen that under the application of electric field the slope of the distribution decreases, indicating an increase in the disorder in the local mode kinetic energies. In other words, the excess entropy due to the dipoles' ordering under electric field is absorbed by the atomic vibrations. Note that this entropy redistribution can also be viewed as "conversion" of spatially inhomogeneous dipole distribution into spatially inhomogeneous temperature distribution. The increased disorder in the energies associated with atomic vibrations explains the increase in the observed temperature. The same data in ferroelectric phase ($T=190$ K) are given in Figs. 4(b) and 4(d). Here we can see only a moderate change in the dipoles' ordering under application of electric field [Fig. 4(b)] accompanied by a moderate increase in the disorder in the demon energies [Fig. 4(d)]. This relatively small redistribution of the entropies explains why ECE is smaller in ferroelectric phase when compared to the ferroelectric phase. Our data indicate that the ability of dipoles to reorder under application of electric field is different for paraelectric

and ferroelectric phases which explains the observed asymmetry in ΔT with respect to T_C .

In summary, we have proposed a computational scheme that allows accurate and efficient atomistic simulations of the electrocaloric effect in ferroelectrics. Applications of this technique to BST alloys in different atomistic configurations has revealed the following: (1) extremely high intrinsic electrocaloric response (15 K per electric field change of 500 kV/cm) in this alloys at room temperature; (2) asymmetry in the dependence of ΔT on ΔE with respect to T_C with very high and nearly constant $\Delta T/\Delta E$ in paraelectric phase and; (3) atomistic mechanism responsible for the enhancement of ECE in paraelectric phase.²⁰ These findings may have very important technological applications since a large range of BST alloys have T_C at or below room temperature.

The authors would like to acknowledge the use of the services provided by Research Computing, University of South Florida. S.L. acknowledges the support from the University of South Florida under Grant No. R074021.

*slisenk@cas.usf.edu

¹A. Mischenko, Q. Zhang, J. Scott, R. Whatmore, and N. Mathur, *Science* **311**, 1270 (2006).

²B. Neese, B. Chu, S.-G. Lu, Y. Wang, E. Furman, and Q. Zhang, *Science* **321**, 821 (2008).

³B. A. Tuttle and D. A. Payne, *Ferroelectrics* **37**, 603 (1981).

⁴P. D. Thacher, *J. Appl. Phys.* **39**, 1996 (1968).

⁵W. N. Lawless, *Phys. Rev. B* **16**, 433 (1977).

⁶B. A. Strukov, *Sov. Phys. Crystallogr.* **11**, 757 (1967).

⁷G. Akcay, S. P. Alpay, J. V. Mantese, and G. A. Rossetti, Jr., *Appl. Phys. Lett.* **90**, 252909 (2007).

⁸S. Prosandeev, I. Ponomareva, and L. Bellaiche, *Phys. Rev. B* **78**, 052103 (2008).

⁹Our convergence tests with respect to the simulation cell size show that $12 \times 12 \times 12$ cell already provides convergent results for disordered system. However, since the largest period along the z direction for the structures studied is 21 we use $12 \times 12 \times 21$ supercell for all structures.

¹⁰L. Walizer, S. Lisenkov, and L. Bellaiche, *Phys. Rev. B* **73**, 144105 (2006).

¹¹A. García and D. Vanderbilt, in *First-Principles Calculations for Ferroelectrics*, Fifth Williamsburg Workshop, edited by R. Cohen and AIP (Woodbury, New York, 1998), p. 54.

¹²In case of $(\text{Ba}_{0.5}\text{Sr}_{0.5})\text{TiO}_3$ solid solution the effective Hamiltonian predicts transition from cubic paraelectric phase to tetragonal ferroelectric phase at $235 \text{ K} \pm 5 \text{ K}$ (220–250 K), from tetragonal to orthorhombic phase at $180 \text{ K} \pm 5 \text{ K}$ (180 K), and

from orthorhombic to rhombohedral phase at $155 \text{ K} \pm 5 \text{ K}$ (140 K).¹⁰ The data in brackets indicate the experimental value for the same transition.

¹³S. Lisenkov and L. Bellaiche, *Phys. Rev. B* **76**, 020102(R) (2007).

¹⁴I. Ponomareva, L. Bellaiche, T. Ostapchuk, J. Hlinka, and J. Petzelt, *Phys. Rev. B* **77**, 012102 (2008).

¹⁵J. Hlinka, T. Ostapchuk, D. Nuzhnyy, J. Petzelt, P. Kuzel, C. Kadlec, P. Vanek, I. Ponomareva, and L. Bellaiche, *Phys. Rev. Lett.* **101**, 167402 (2008).

¹⁶S. Lisenkov, I. Ponomareva, and L. Bellaiche, *Phys. Rev. B* **79**, 024101 (2009).

¹⁷N. Metropolis, A. Rosenbluth, M. Rosenbluth, and A. Teller, *J. Chem. Phys.* **21**, 1087 (1953).

¹⁸M. Creutz, *Phys. Rev. Lett.* **50**, 1411 (1983).

¹⁹F. Jona and G. Shirane, *Ferroelectric Crystals* (McMillan, New York, 1962).

²⁰Such features appear to be general for a wide range of Ba concentrations as obtained from additional computations for BST alloys with Ba concentration of 60% and 40%. The magnitude of electrocaloric response, however, may depend on Ba concentration. For example, increasing Ba concentration from 50% to 60% resulted in $\approx 10\%$ increase in ΔT at T_C under applied electric field of 500 kV/cm, while decreasing Ba concentration from 50% to 40% resulted in $\approx 5\%$ decrease in ΔT at T_C under same applied field.